Journal of the Physical Society of Japan **86**, 011010 (2017)
https://doi.org/10.7566/JPSJ.86.011010

Thermal Hall Effect of Magnons

Shuichi Murakami[1,2,3*] and Akihiro Okamoto[1]

[1]*Department of Physics, Tokyo Institute of Technology, Meguro, Tokyo 152-8551, Japan*
[2]*TIES, Tokyo Institute of Technology, Meguro, Tokyo 152-8551, Japan*
[3]*CREST, Tokyo Institute of Technology, Meguro, Tokyo 152-8551, Japan*

(Received September 7, 2016; accepted October 21, 2016; published online December 8, 2016)

We review recent developments in theories and experiments on the magnon Hall effect. We derive the thermal Hall conductivity of magnons in terms of the Berry curvature of magnonic bands. In addition to the Dzyaloshinskii–Moriya interaction, we show that the dipolar interaction can make the Berry curvature nonzero. We mainly discuss theoretical aspects of the magnon Hall effect and related theoretical works. Experimental progress in this field is also mentioned.

1. Introduction

Magnon (spin wave) is a low-energy collective excitation in magnets.[1,2] Magnon attracts much attention in the field of spintronics,[3,4] and nowadays leads us to a new field of physics, called "magnonics".[5–8] Magnonics aims to control and process information using magnons, and a number of magnonic devices have been proposed. For these purposes, the basic understanding of the properties of magnons and the precise control of magnons in magnets are urgently called for. Particularly in insulating magnets such as yttrium-iron-garnet (YIG), magnons can carry spin information for a long distance of centimeter order without dissipation by Joule heating.[9] The magnon current can be experimentally generated by the spin Hall effect,[10] and its motion can be observed by the time- and space-resolved measurement methods.[11]

We discuss the thermal Hall effect of magnons in this review article, as an example of various Hall effects driven by the Berry curvature in $\mathbf{k}$ space. The Berry curvature is defined in differential geometry, characterizing how rapid the wavefunction changes as a function of the wavevector $\mathbf{k}$, and it appears in a wide range of wave phenomena. It is associated with the band structure in $\mathbf{k}$ space. Historically, the Berry curvature in $\mathbf{k}$ space was first considered in the electronic band structure in solids,[12–15] and then it has been applied to other types of particle systems such as magnons[16–18] and photons.[19] Let us take electronic systems as an example. In solid crystals, electronic eigenenergies form a band structure in $\mathbf{k}$ space due to their spatial periodicity. Bloch eigenstates turn out to have nontrivial mathematical structure in $\mathbf{k}$ space characterized by the Berry curvature, and the Berry curvature manifests itself in the dynamics of the particle. For example, for magnons in a magnet, a temperature gradient will induce a transverse heat current through the Berry curvature (see Fig. 1), in addition to the usual longitudinal heat current. This generation of transverse heat current is called a thermal Hall effect. As we discuss later, this magnon thermal Hall effect can potentially be a new probe for the physical properties of magnets.

This Berry curvature has been discussed in the context of the anomalous Hall effect since the 1970s. At that time, it was not called Berry curvature, and through the seminal paper by Berry in 1984[20] and subsequent works, its mathematical properties and roles in physical phenomena have been clarified. For example, the Berry curvature leads to various Hall effect, such as anomalous Hall and spin Hall effects.

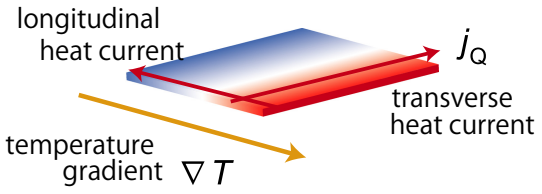

Fig. 1. (Color online) Schematic figure of the thermal Hall effect.

Moreover, theoretical and experimental research studies in the field of quantum Hall effect and topological insulators have revealed that the Berry curvature leads to various topological phases.

In this paper, we review various applications of the Berry curvature for magnons, particularly to the thermal Hall effect of magnons. The properties of magnons largely depend on the details of the material itself, such as crystal structure and magnetic interactions between spins. In the following, we focus on magnons in ferromagnets for simplicity, and use a bosonic description of magnons. The results explained in the following can be easily extended to general magnets, as long as magnetic excitations are expressed as bosons. Throughout this paper, we consider magnetic insulators for simplicity, because theoretical analysis consequently becomes simpler. We also assume that magnons do not interact with each other.

This paper is organized as follows. In Sect. 2 the Berry phase dynamics of electrons and its applications to magnons are reviewed. In Sect. 3, theories of the magnon Hall effect are explained in detail, and the applications of such an effect to magnetostatic waves are discussed in Sect. 4. In Sect. 5 we summarize the paper and discuss related experiments and theories on this effect.

2. Wavepacket Dynamics by the Berry Curvature

2.1 *Berry curvature dynamics of electrons*

First, we begin with the Berry curvature dynamics of electrons, such as the spin Hall effect of electrons. Let $\psi_{n\mathbf{k}}(\mathbf{r}) = u_n(\mathbf{k},\mathbf{r})e^{i\mathbf{k}\cdot\mathbf{r}}$ denote the electronic Bloch wavefunction, where n is the band index. Although this Bloch wavefunction is spatially extended, one can construct a wavepacket as a linear combination of Bloch waves, and it is localized both in $\mathbf{k}$ space and $\mathbf{r}$ space to some extent. The central positions in $\mathbf{k}$ and $\mathbf{r}$ spaces evolve with time, as described by the following semiclassical equations of motion,[12,13,15]

$$\dot{\mathbf{r}} = \frac{1}{\hbar}\frac{\partial E_n(\mathbf{k})}{\partial \mathbf{k}} - \dot{\mathbf{k}} \times \mathbf{\Omega}_n(\mathbf{k}), \tag{1}$$

$$\hbar\dot{\mathbf{k}} = -e\mathbf{E}. \tag{2}$$

Here, E_n is the energy of the nth eigenstate, $\mathbf{E}$ is an electric field, $-e$ is the electron charge, and $\mathbf{\Omega}_n(\mathbf{k}) \equiv i\langle \frac{\partial u_n}{\partial \mathbf{k}} | \times | \frac{\partial u_n}{\partial \mathbf{k}} \rangle$ is called a Berry curvature.[20] The second term of the right-hand side of Eq. (1) is called anomalous velocity. This anomalous velocity is perpendicular to the applied electric field, and thus leads to a Hall effect. For example, from this semiclassical equation of motion, we obtain the Hall conductivity in two-dimensional systems as

$$\sigma_{xy} = -\frac{e^2}{h}\sum_n \int_{\mathrm{BZ}} \frac{d^2\mathbf{k}}{2\pi}\Omega_{n,z}(\mathbf{k})\rho^{\mathrm{F}}(E_n(\mathbf{k})), \tag{3}$$

where $\rho^{\mathrm{F}}(E)$ is the Fermi distribution function. Note that Eq. (3) is identical to that obtained using the Kubo formula in the linear response theory.[12,14]

In addition to the Hall effect described here, the Berry curvature in $\mathbf{k}$ space leads to variants of the Hall effect, such as the spin Hall effect.[21,22] In a nonmagnetic material, the Berry curvature $\mathbf{\Omega}_n(\mathbf{k})$ has opposite signs for opposite spins, if the material has a spin–orbit interaction (SOI). Therefore, an electric field induces a spin current perpendicular to the field due to the anomalous velocity; this is called the spin Hall effect.

The Berry curvature also leads to various topological phases. For example, if we consider a two-dimensional band insulator at zero temperature, we have

$$\sigma_{xy} = -\frac{e^2}{h}\sum_{n\in \mathrm{occ.}} Ch_n, \quad Ch_n \equiv \int_{\mathrm{BZ}} \frac{d^2\mathbf{k}}{2\pi}\Omega_{n,z}(\mathbf{k}), \tag{4}$$

where the summation is taken over the occupied bands. The quantity Ch_n is called a Chern number, which is known to take an integer value (when the nth band is separated from other bands by a gap).[14,23] Therefore, σ_{xy} is an integer multiple of e^2/h and it corresponds to the integer quantum Hall effect if this σ_{xy} is nonzero in a band insulator.

2.2 *Berry curvature dynamics of magnons: Overview of the magnon Hall effect*

According to the semiclassical equation of motion for electrons, Eq. (1), the effect of the Berry curvature appears when $\dot{\mathbf{k}}$ becomes nonzero, and $\dot{\mathbf{k}}$ is equal to the external force times $\hbar^{-1}$. Thus, when a force is exerted to accelerate an electron, it will undergo a transverse shift perpendicular to the force, giving rise to the Hall effect. This picture applies also to other particles or quasiparticles having a wave nature. Whenever an external force is exerted on a particle, a Hall effect appears in general, owing to the Berry curvature (if not prohibited by symmetry). In the case of the Hall effect of light, as an example, a spatial gradient of the refractive index serves an "external force" applied to a photon wavepacket, and induces a transverse shift.[19,24]

For the magnons, one can consider several possibilities for this external force. Theoretical treatment becomes excellent and universal when we take a temperature gradient as this external force. Other external perturbations, such as a magnetic field gradient, will drive the magnons, but a magnetic field gradient affects the magnons in a complex way, and it is not possible to have a unified formula applicable to a wide range of magnets. For this reason, we consider here the Hall effect of magnons by a temperature gradient, i.e., the thermal Hall effect of magnons.

The thermal Hall effect of magnons was predicted theoretically by Katsura et al.[16] They calculated thermal Hall conductivity using the Kubo formula and showed that the thermal Hall effect indeed arises owing to the Berry curvature in $\mathbf{k}$ space, associated with magnon wavefunctions. They also showed that the Dyaloshinskii–Moriya (DM) interaction makes the Berry curvature nonzero. Then, Onose et al.[17] measured the thermal Hall effect in an insulating ferromagnet $Lu_2V_2O_7$ having exchange and DM interactions, and compared the obtained data with theoretical results. On the other hand, Matsumoto and Murakami found[18,25] that there should be a correction term to the thermal Hall conductivity found in Ref. 16; the result in Refs. 18 and 25 was derived by two independent methods, the linear response theory and the semiclassical theory of Berry curvature dynamics, which give identical results. They also showed that the dipolar interaction can also give a nonzero Berry curvature. In the following section, we explain these theoretical frameworks.

3. Theories of the Magnon Hall Effect

By the Holstein–Primakoff transformation, the magnon excitations are shown to obey boson statistics. As is similar to the electronic Hall effect, the Berry curvature term induces a transverse magnon current perpendicular to a temperature gradient, which corresponds to the Nernst effect. This magnon current is a magnon number current, i.e., a flow of the number of magnons per unit time. Nevertheless, it is not easy to experimentally measure this magnon number current because of the following two reasons. First, the magnon number is well defined only when some spin component, e.g., s_z, is conserved, but it is not the case in general. In the bosonic description of magnons, the bosonic Hamiltonian is a bilinear form of the creation operator $b^\dagger$ and the annihilation operator b, if we neglect interaction terms between magnons. Nonetheless, the Hamiltonian generally takes the Bogoliubov–de Gennes (BdG) form involving $b^\dagger b^\dagger$ or bb terms. In such cases, the number of bosons is not conserved and the magnon number current is ill-defined. Second, in reality, magnon–magnon interactions always exist, and they violate the conservation of the magnon number. Thus, in such cases, the number of bosons and the magnon number current cannot be measured as well-defined quantities. Because of these reasons, we consider the heat current of magnons instead of the magnon number current.

In contrast to the magnon number current discussed above, the heat current is always well defined because of the energy conservation. Thus, here, we consider the thermal Hall effect of magnons, where the temperature gradient induces a transverse heat current. In order to calculate the thermal Hall effect, we write down the linear response of the system in the following way, in analogy with the electron system,[26–31]

$$\mathbf{j} = L_{11}[-\nabla U - \nabla\mu] + L_{12}\left[T\nabla\left(\frac{1}{T}\right)\right], \tag{5}$$

$$\mathbf{j}_{\mathrm{Q}} = L_{12}[-\nabla U - \nabla\mu] + L_{22}\left[T\nabla\left(\frac{1}{T}\right)\right], \tag{6}$$

where L_{ij} are tensors, the heat current density is defined as $\mathbf{j}_{\rm Q} \equiv \mathbf{j}_{\rm E} - \mu\mathbf{j}$, $\mathbf{j}_{\rm E}$ is the energy current density, $\mathbf{j}$ is the magnon current density, U is a potential for magnons, and μ is the magnon chemical potential. The Onsager reciprocity is expressed as $L_{12} = L_{21}$. Concerning the off-diagonal elements in the spatial index, L_{11}^{xy} represents the Hall effect, $L_{12}^{xy} = L_{21}^{xy}$ represents the Nernst–Ettinghausen effect, and L_{22}^{xy} represents the thermal Hall effect. In the following, we calculate the thermal Hall effect by two methods, the semiclassical theory and the linear response theory, to show that they give identical results.[18,25)]

3.1 *Semiclassical equations of motions for magnons*

The above semiclassical description in Eqs. (1) and (2) is based on the wave nature of electrons. Therefore, we can consider an analogous pheonomenon for magnons by constructing a similar framework. The semiclassical equations of motion for magnons are described as[18,25)]

$$\dot{\mathbf{r}} = \frac{1}{\hbar}\frac{\partial \varepsilon_{n\mathbf{k}}}{\partial \mathbf{k}} - \dot{\mathbf{k}} \times \mathbf{\Omega}_n(\mathbf{k}), \tag{7}$$

$$\hbar\dot{\mathbf{k}} = -\nabla U(\mathbf{r}). \tag{8}$$

Here, n is the band index, $\varepsilon_{n\mathbf{k}}$ is the energy of the magnon in the nth band, and $\mathbf{\Omega}_n(\mathbf{k})$ is the Berry curvature in $\mathbf{k}$ space, defined from the magnon Bloch wavefunctions. We put by hand a potential term $U(\mathbf{r})$ for magnons here. From now on, we restrict ourselves to two-dimensional magnets, while generalizations to three dimensions are straightforward. Then, the wavevector $\mathbf{k} = (k_x, k_y)$ is along the xy-plane, and the Berry curvature $\mathbf{\Omega}_n(\mathbf{k})$ is along the z-axis.

We now consider magnon transport under the temperature gradient. The temperature gradient gives rise to the spatial variation of magnon density. Nevertheless, we cannot incorporate the temperature gradient into Eq. (8) as the potential U because it affects the magnon physics via the Boltzmann factor $e^{-E/(k_{\rm B}T)}$, and thus the effect of temperature depends on the magnon energy. Therefore, we take a different route.

First, note that, at the edges of the magnet, there is a potential gradient that confines the magnons inside the magnet. Therefore, the confinement potential $U(\mathbf{r})$ changes from zero to infinity as the position $\mathbf{r}$ changes from inside the magnet to the outside. Thus, $\dot{\mathbf{k}}$ in Eq. (8) is pointing inward near the edges of the magnet, and thus, the anomalous velocity [the second term of the r.h.s. of Eq. (7)] is along the edge of the magnet, forming an edge current of magnons [Fig. 2(a)]. The magnon edge current I and the edge energy current $I^{\rm E}$ are expressed as

$$I = -\frac{1}{\hbar V}\sum_{n,\mathbf{k}}\int_{\varepsilon_{n\mathbf{k}}}^{\infty} d\varepsilon\, \rho^{\rm B}(\varepsilon)\Omega_{n,z}(\mathbf{k}), \tag{9}$$

$$I^{\rm E} = -\frac{1}{\hbar V}\sum_{n,\mathbf{k}}\int_{\varepsilon_{n\mathbf{k}}}^{\infty} d\varepsilon\, \varepsilon\rho^{\rm B}(\varepsilon)\Omega_{n,z}(\mathbf{k}), \tag{10}$$

where V is the area of the sample, $\rho^{\rm B}(\varepsilon)$ is the Bose distribution function $\rho^{\rm B}(\varepsilon) = (e^{\beta(\varepsilon-\mu)} - 1)^{-1}$, $\beta = 1/(k_{\rm B}T)$, $k_{\rm B}$ is the Boltzmann constant, μ is the chemical potential, and T is the temperature. Henceforth, the magnon current means the current of the magnon number.

If we divide the magnet into small regions, each of which has a confining potential at the edge, there will be edge currents along the edges of the individual small regions of the magnet. Then, by regarding the entire magnet as a collection of these small magnets, the edge currents in individual small regions cancel each other in the bulk, leaving behind the magnon current along the edge of the entire system. This idea of dividing the magnet into small regions is useful for incorporating the spatial gradient of temperature or chemical potential. When the gradient of the chemical potential μ or temperature T is present, the edge magnon currents in the individual regions are different, and do not cancel between neighboring regions. As a result, the transverse magnon current perpendicular to the temperature gradient is generated [Fig. 2(c)]. This indicates the magnon Hall effect. Therefore, the transverse magnon current density $\mathbf{j}$ and the transverse energy current density $\mathbf{j}_{\rm E}$ are written as

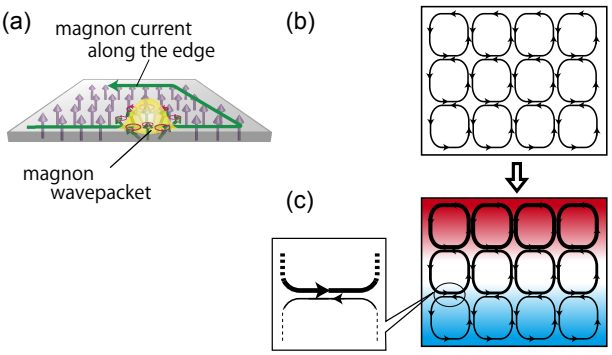

Fig. 2. (Color online) (a) Schematic of the magnon edge current. (b) Magnet in equilibrium, which is divided into small regions. The magnon edge currents within the neighboring regions cancel each other. (c) Magnet with the temperature gradient. The magnon edge currents in the small regions do not cancel, leading to a net transverse current.

$$\mathbf{j} = \nabla \times \frac{1}{\hbar V}\sum_{n,\mathbf{k}}\int_{\varepsilon_{n\mathbf{k}}}^{\infty} \rho^{\rm B}(\varepsilon)\mathbf{\Omega}_n(\mathbf{k})\, d\varepsilon, \tag{11}$$

$$\mathbf{j}_{\rm E} = \nabla \times \frac{1}{\hbar V}\sum_{n,\mathbf{k}}\int_{\varepsilon_{n\mathbf{k}}}^{\infty} \varepsilon\rho^{\rm B}(\varepsilon)\mathbf{\Omega}_n(\mathbf{k})\, d\varepsilon. \tag{12}$$

From Eqs. (11) and (12), we can derive various transverse transport coefficients. For instance, in the presence of the temperature gradient in the y-direction, the edge current and energy current density in the x-direction are written as

$$(j)_x^{\nabla T} = T\partial_y\left(\frac{1}{T}\right)\sum_{n,\mathbf{k}}\int_{\varepsilon_{n\mathbf{k}}}^{\infty} \frac{\varepsilon-\mu}{\hbar V}\left(\frac{d\rho^{\rm B}}{d\varepsilon}\right)\Omega_{n,z}(\mathbf{k})\, d\varepsilon, \tag{13}$$

$$(j_{\rm E})_x^{\nabla T} = T\partial_y\left(\frac{1}{T}\right)\sum_{n,\mathbf{k}}\int_{\varepsilon_{n\mathbf{k}}}^{\infty} \frac{\varepsilon(\varepsilon-\mu)}{\hbar V}\left(\frac{d\rho^{\rm B}}{d\varepsilon}\right)\Omega_{n,z}(\mathbf{k})\, d\varepsilon. \tag{14}$$

Similarly, we obtain these currents in the presence of the gradient of the chemical potential in the y-direction:

$$(j)_x^{\nabla\mu} = -\partial_y\mu\,\frac{1}{\hbar V}\sum_{n,\mathbf{k}}\int_{\varepsilon_{n\mathbf{k}}}^{\infty} \left(\frac{d\rho^{\rm B}}{d\varepsilon}\right)\Omega_{n,z}(\mathbf{k})\, d\varepsilon, \tag{15}$$

$$(j_{\rm E})_x^{\nabla\mu} = -\partial_y\mu\,\frac{1}{\hbar V}\sum_{n,\mathbf{k}}\int_{\varepsilon_{n\mathbf{k}}}^{\infty} \varepsilon\left(\frac{d\rho^{\rm B}}{d\varepsilon}\right)\Omega_{n,z}(\mathbf{k})\, d\varepsilon. \tag{16}$$

By calculating the heat current as $\mathbf{j}_{\rm Q} \equiv \mathbf{j}_{\rm E} - \mu\mathbf{j}$, we can derive the transverse transport coefficients L_{ij}^{xy} in Eqs. (5) and (6) as

$$L_{ij}^{xy} = -\frac{1}{\hbar V\beta^q}\sum_{n,\mathbf{k}}\Omega_{n,z}(\mathbf{k})c_q(\rho_n^{\rm B}), \tag{17}$$

where $i,j = 1,2$, $c_q(\rho_n^{\rm B}) = \int_{\varepsilon_{n\mathbf{k}}}^{\infty} d\varepsilon(\beta(\varepsilon-\mu))^q(-\frac{d\rho^{\rm B}}{d\varepsilon}) = \int_0^{\rho_n^{\rm B}}(\log(1+t^{-1}))^q\, dt$, $q = i+j-2$, and $\rho_n^{\rm B} \equiv \rho^{\rm B}(\varepsilon_{n\mathbf{k}})$. Here,

$\log(1+t^{-1})$ is the inverse of the Bose distribution function; for fermions, this factor $\log(1+t^{-1})$ is replaced by $\log(-1+t^{-1})$. For example, $c_0(\rho^{\rm B})=\rho^{\rm B}$, $c_1(\rho^{\rm B})=(1+\rho^{\rm B})\log(1+\rho^{\rm B})-\rho^{\rm B}\log\rho^{\rm B}$, and $c_2(\rho^{\rm B})=(1+\rho^{\rm B})(\log\frac{1+\rho^{\rm B}}{\rho^{\rm B}})^2-(\log\rho^{\rm B})^2-2{\rm Li}_2(-\rho^{\rm B})$, where ${\rm Li}_2(z)$ is the polylogarithm function. In particular, the thermal Hall conductivity in a clean limit is

$$\kappa^{xy}=L_{22}^{xy}/T=-\frac{k_{\rm B}^2T}{\hbar V}\sum_{n,\mathbf{k}}c_2(\rho^{\rm B}(\varepsilon_{n\mathbf{k}}))\Omega_{n,z}(\mathbf{k}). \tag{18}$$

Thus, the contribution of each magnon state to the thermal Hall effect is proportional to the Berry curvature.

3.2 Linear response theory

In order to calculate transport coefficients within the linear response theory, we first note two types of forces as an external field. In Eqs. (5) and (6), the term ∇U is a dynamical force, exerting a force on a particle. On the other hand, $\nabla\mu$ and $\nabla(1/T)$ are called statistical forces because these terms give rise to a spatial difference in particle distribution, which drives the particle current.

For a statistical force, one can consider a corresponding dynamical force, and vice versa. To explain this, we take an example for electrons; the electric field is a dynamical force, while the gradient of the chemical potential is a statistical force. They are known to enter the linear response theory together, as an electrochemical potential $-eV+\mu$. The thermal Hall conductivity is defined as a response to a statistical force ∇T, while the standard linear response theory can only deal with dynamical forces. Therefore, we add by hand a dynamical force $\nabla\chi$, which corresponds to the statistical force $T\nabla(\frac{1}{T})$;

$$\mathbf{j}=L_{11}[-\nabla U-\nabla\mu]+L_{12}\left[-\nabla\chi+T\nabla\left(\frac{1}{T}\right)\right], \tag{19}$$

$$\mathbf{j}_{\rm Q}=L_{12}[-\nabla U-\nabla\mu]+L_{22}\left[-\nabla\chi+T\nabla\left(\frac{1}{T}\right)\right]. \tag{20}$$

This $\nabla\chi$ term is called a pseudogravitational potential as first introduced by Luttinger.[32] Here, the perturbation χ adds to the Hamiltonian H the term χH as $H'\equiv(1+\chi)H=H+\chi H$, and its spatial gradient $\nabla\chi$ exerts a force proportional to the energy of the particle. For this perturbation $\nabla\chi$, we can proceed as in the standard linear response theory.

By adding the perturbations U and χ, the perturbation term is written as $H'=\sum_j U(\mathbf{r}_j)+\frac{1}{2}\{H,\sum_j\chi(\mathbf{r}_j)\}$ within the first-quantized form, where $\mathbf{r}_j$ is the position of the jth magnon, H is the unperturbed Hamiltonian, and $\{\hat{A},\hat{B}\}=\hat{A}\hat{B}+\hat{B}\hat{A}$ represents the anticommutator. In equilibrium, the magnon current density and energy current density are written as

$$\mathbf{j}^{(0)}(\mathbf{r})=\frac{1}{2}\sum_j\{\mathbf{v}_j,\delta(\mathbf{r}-\mathbf{r}_j)\},$$

$$\mathbf{j}_{\rm E}^{(0)}(\mathbf{r})=\frac{1}{2}\{H,\mathbf{j}^{(0)}(\mathbf{r})\}, \tag{21}$$

where $\mathbf{v}_j$ is the velocity operator of the jth magnon. One should be cautious in that the operators of the magnon and heat currents acquire additional terms, when the perturbation is added. Correspondingly, the thermal transport coefficients consist of two parts: $L_{ij}^{\alpha\beta}=S_{ij}^{\alpha\beta}+M_{ij}^{\alpha\beta}$. Here, $\alpha,\beta=x,y$, $i,j=1,2$. The deviation of the density matrix from equilibrium generates $S_{ij}^{\alpha\beta}$, which is calculated using the Kubo formula, expressed as a current–current correlation function. The deviation of the current operator due to external fields generates $M_{ij}^{\alpha\beta}$. The latter term $M_{ij}^{\alpha\beta}$ is not of the form of a correlation function, but of an expectation value of the orbital angular momentum or the like. In the clean limit, the transverse response coefficients ($\alpha\neq\beta$) are expressed as

$$S_{ij}^{\alpha\beta}=\frac{i\hbar}{V}\int\rho^{\rm B}(\eta)\,{\rm Tr}\left(j_i^\alpha\frac{dG^+}{d\eta}j_j^\beta\delta(\eta-H)-j_i^\alpha\delta(\eta-H)j_j^\beta\frac{dG^-}{d\eta}\right)d\eta,\quad(i,j=1,2), \tag{22}$$

$$M_{11}^{\alpha\beta}=0, \tag{23}$$

$$M_{12}^{\alpha\beta}=\frac{1}{2V}\int\rho^{\rm B}(\eta)\,{\rm Tr}[\delta(\eta-H)(r^\alpha v^\beta-r^\beta v^\alpha)]\,d\eta, \tag{24}$$

$$M_{22}^{\alpha\beta}=\frac{1}{V}\int\eta\rho^{\rm B}(\eta)\,{\rm Tr}\,\delta(\eta-H)(r^\alpha v^\beta-r^\beta v^\alpha)\,d\eta+\frac{i\hbar}{4V}\int\rho^{\rm B}(\eta)\,{\rm Tr}\,\delta(\eta-H)[v^\alpha,v^\beta]\,d\eta. \tag{25}$$

Here, $G^\pm$ is the Green's function $G^\pm(\eta)=(\eta-H\pm i\epsilon)^{-1}$ with ϵ being the positive infinitesimal, $\mathbf{j}_1=\mathbf{v}$, $\mathbf{j}_2=\frac{1}{2}(H\mathbf{v}+\mathbf{v}H)$, and $\mathbf{v}$ is the velocity operator. These thermal transport coefficients can be written in terms of the Bloch wavefunctions of magnons $u_n(\mathbf{k})$:

$$S_{ij}^{\alpha\beta}=\frac{2}{\hbar V}{\rm Im}\sum_{n,\mathbf{k}}\rho_n^{\rm B}\left\langle\frac{\partial u_n}{\partial k_\alpha}\middle|\left(\frac{H+\varepsilon_{n\mathbf{k}}}{2}\right)^q\middle|\frac{\partial u_n}{\partial k_\beta}\right\rangle, \tag{26}$$

$$M_{ij}^{\alpha\beta}=-S_{ij}^{\alpha\beta}+\frac{2(k_{\rm B}T)^q}{\hbar V}{\rm Im}\sum_{n,\mathbf{k}}c_q(\rho_n^{\rm B})\left\langle\frac{\partial u_n}{\partial k_\alpha}\middle|\frac{\partial u_n}{\partial k_\beta}\right\rangle, \tag{27}$$

where $q=i+j-2$. Here, we have taken $\mu=0$ for simplicity, since the magnon number is not conserved in general. Thus, the total thermal transport coefficients are written as

$$L_{ij}^{\alpha\beta}=S_{ij}^{\alpha\beta}+M_{ij}^{\alpha\beta}=-\frac{(k_{\rm B}T)^q}{\hbar V}\sum_{n,\mathbf{k}}\Omega_{n,z}(\mathbf{k})c_q(\rho_n^{\rm B}), \tag{28}$$

which agrees with the results from the semiclassical theory, Eq. (17). This result was also derived in Ref. 33 by constructing a systematic approach for thermal transport coefficients while introducing a notion of energy magnetization.

Historically, for the thermal Hall effect, the contribution from $S_{22}^{\alpha\beta}$ was calculated in Refs. 16 and 17; later, the other contribution from $M_{22}^{\alpha\beta}$ was calculated in Refs. 18 and 25, to obtain the correct result Eq. (18). This result roughly agrees with the experimental data in Ref. 17 for the ferromagnetic Mott insulator $Lu_2V_2O_7$. Note that the latter contribution (M_{ij}) is from the orbital motion of magnons. It is nonzero for the Nernst effect (M_{12}) and the thermal Hall effect (M_{22}), while it vanishes for the Hall effect (M_{11}) from Eq. (27). Therefore, the Hall conductivity is expressed solely as a current–current correlation function.

We comment on another aspect of the theoretical treatment of heat transport. In the standard calculation of the linear response of electrons to the electric field, there are two equivalent ways to incorporate the electric field: (i) as a vector potential or (ii) as a scalar potential. In textbooks on solid-state physics, the standard way is to use (i) the vector potential, but (ii) is also possible and gives the same results.

In the case of magnons, the response to ∇U or $\nabla\mu$ corresponds to (ii) the scalar potential. Moreover, the theoretical framework of (i) the vector potential to calculate the response to the temperature gradient has been formulated in Ref. 34.

3.3 *BdG Hamiltonian for bosons*

In some magnets, the magnon Hamiltonian takes the form of the BdG Hamiltonian, and it does not conserve the magnon number. In such cases, the magnon current $\mathbf{j}$ is ill-defined, and a response to ∇U, which is a potential to a single magnon, is also ill-defined. Thus, the linear response takes the form

$$\mathbf{j}_{\mathrm{Q}} = L_{22}\left[-\nabla\chi + T\nabla\left(\frac{1}{T}\right)\right]. \tag{29}$$

The theory of the Berry curvature and the magnon thermal Hall effect for such cases[35–38] is formulated similarly to that of the Hall effect in superconductors for electrons.[39–41]

We begin with the magnon BdG Hamiltonian:

$$\mathcal{H} = \frac{1}{2}\sum_{\mathbf{k}}(\beta_{\mathbf{k}}^{\dagger}\beta_{-\mathbf{k}})H_{\mathbf{k}}\begin{pmatrix}\beta_{\mathbf{k}}\\ \beta_{-\mathbf{k}}^{\dagger}\end{pmatrix}, \tag{30}$$

where $\beta_{\mathbf{k}}^{\dagger} = (\beta_{1,\mathbf{k}}^{\dagger},\ldots,\beta_{N,\mathbf{k}}^{\dagger})$. $\beta_{i,\mathbf{k}}$ $(1 \le i \le N)$ are the bosonic (magnon) annihilation operators, $[\beta_{i,\mathbf{k}}, \beta_{j,\mathbf{k}'}^{\dagger}] = \delta_{\mathbf{k}\mathbf{k}'}\delta_{ij}$, and N is the number of magnon bands. The particle–particle pairing terms, $\beta_i^{\dagger}\beta_j^{\dagger}$ or $\beta_i\beta_j$, violate the conservation of the total number of magnons. The BdG Hamiltonian is diagonalized by a $(2N)\times(2N)$ para-unitary matrix $T_{\mathbf{k}}$,[42] which is regarded as a bosonic version of the Bogoliubov transformation.

$$\begin{aligned}\mathcal{H} &= \frac{1}{2}\sum_{\mathbf{k}}(\gamma_{\mathbf{k}}^{\dagger}\gamma_{-\mathbf{k}})\mathcal{E}_{\mathbf{k}}\begin{pmatrix}\gamma_{\mathbf{k}}\\ \gamma_{-\mathbf{k}}^{\dagger}\end{pmatrix}\\ &= \sum_{\mathbf{k}}\sum_{n=1}^{N}\varepsilon_{n\mathbf{k}}\left(\gamma_{n\mathbf{k}}^{\dagger}\gamma_{n\mathbf{k}} + \frac{1}{2}\right),\end{aligned} \tag{31}$$

where $\gamma_{\mathbf{k}}^{\dagger} = (\gamma_{1,\mathbf{k}}^{\dagger},\ldots,\gamma_{N,\mathbf{k}}^{\dagger})$ with the bosonic annihilation operators $\gamma_{i\mathbf{k}}$, and

$$\begin{pmatrix}\gamma_{\mathbf{k}}\\ \gamma_{-\mathbf{k}}^{\dagger}\end{pmatrix} = T_{\mathbf{k}}^{-1}\begin{pmatrix}\beta_{\mathbf{k}}\\ \beta_{-\mathbf{k}}^{\dagger}\end{pmatrix}, \tag{32}$$

$$\mathcal{E}_{\mathbf{k}} = T_{\mathbf{k}}^{\dagger}H_{\mathbf{k}}T_{\mathbf{k}} = \mathrm{diag}(\varepsilon_{1\mathbf{k}},\ldots,\varepsilon_{N\mathbf{k}},\varepsilon_{1,-\mathbf{k}},\ldots,\varepsilon_{N,-\mathbf{k}}). \tag{33}$$

The boson commutation relation for $\gamma_{\mathbf{k}}$ requires that $T_{\mathbf{k}}$ must satisfy the para-unitary conditions,

$$T_{\mathbf{k}}^{\dagger}\sigma_3 T_{\mathbf{k}} = \sigma_3 = T_{\mathbf{k}}\sigma_3 T_{\mathbf{k}}^{\dagger}, \quad \sigma_3 = \begin{pmatrix}1_{N\times N} & 0\\ 0 & -1_{N\times N}\end{pmatrix}. \tag{34}$$

The temperature gradient is incorporated as a pseudogravitational potential χ, and as in the previous case, the total thermal transport coefficient is the sum of the two contributions: $L_{22} = S_{22} + M_{22}$. As a result, the thermal Hall conductivity is expressed as

$$\kappa_{xy} = \frac{L_{22}^{xy}}{T} = -\frac{k_{\mathrm{B}}^2 T}{\hbar V}\sum_{\mathbf{k}}\sum_{n=1}^{N}\left(c_2(\rho^{\mathrm{B}}(\varepsilon_{n\mathbf{k}})) - \frac{\pi^2}{3}\right)\Omega_{n,z}(\mathbf{k}). \tag{35}$$

$\Omega_{n,z}(\mathbf{k})$ is the Berry curvature in $\mathbf{k}$ momentum space for the BdG Hamiltonian, which is defined as[36]

$$\Omega_{n,z}(\mathbf{k}) \equiv i\epsilon_{\mu\nu z}\left[\sigma_3\frac{\partial T_{\mathbf{k}}^{\dagger}}{\partial k_\mu}\sigma_3\frac{\partial T_{\mathbf{k}}}{\partial k_\nu}\right]_{nn} \quad (n = 1,2,\ldots,2N). \tag{36}$$

Equation (35) is written only with the Berry curvature in particle space: $\mathbf{\Omega}_{n\mathbf{k}}$ $(1 \le n \le N)$, while in antiparticle space, the Berry curvature $(N+1 \le n \le 2N)$ is given by

$$\mathbf{\Omega}_{n+N,-\mathbf{k}} = -\mathbf{\Omega}_{n\mathbf{k}}. \tag{37}$$

This formula comes from the particle–hole symmetry:

$$H_{\mathbf{k}} = \sigma_1(H_{-\mathbf{k}})^{\mathrm{t}}\sigma_1, \quad \sigma_1 = \begin{pmatrix}0 & 1_{N\times N}\\ 1_{N\times N} & 0\end{pmatrix}. \tag{38}$$

If the two-dimensional magnet is spatially periodic, the wavevector $\mathbf{k}$ is restricted within the first Brillouin zone. Then, if there is a gap in the magnon band structure, one can define a Chern number for the set of bands below the gap, similar to the electronic case in Eq. (4) as

$$Ch \equiv \sum_{n}{}' \int_{\mathrm{BZ}} \frac{dk_x\, dk_y}{2\pi}\Omega_{n,z}(\mathbf{k}),$$

where $\sum_n'$ denotes the sum over the bands below the gap, and it is quantized to be an integer.[36–38,43] This integer Chern number represents a number of chiral edge modes within the magnon band gap, as has been theoretically proposed in Refs. 36–38 and 43.

Lastly we note that the spin Nernst effect in an antiferromagnet is theoretically proposed in Refs. 44 and 45, within the bosonic Bogoliubov–de Gennes description explained here. Using a model of an antiferromagnet on a honeycomb lattice in the presence of the DM interaction, it is shown that the temperature gradient gives rise to a transverse magnon current but no heat current, i.e., a spin Nernst effect but no thermal Hall effect.

4. Spin–Spin Interaction for Nonzero Berry Curvature

The theory in the previous section applies to any noninteracting bosonic systems. The Berry curvature can be defined when the system is uniform or periodic in space. Nonetheless, the Berry curvature $\mathbf{\Omega}_n(\mathbf{k}) \equiv i\langle\frac{\partial u_n}{\partial\mathbf{k}}|\times|\frac{\partial u_n}{\partial\mathbf{k}}\rangle$ is not always nonzero and depends on the interactions involved. Roughly speaking, with an analogy to electronic systems, some kind of "spin–orbit interaction" is needed for the nonzero Berry curvature, since otherwise the periodic part of the Bloch wavefunction, u_n, does not depend on $\mathbf{k}$. For example, if the magnet has exchange interaction only, the Berry curvature is zero.

One of the interactions that make the magnon Berry curvature nonzero is the DM interaction,[17,46] which is natural because the DM interaction itself originates from the SOI of electrons. Indeed, the thermal Hall effect appears in the ferromagnet $Lu_2V_2O_7$[17] having the DM interaction and some other magnets.[46] In some magnets despite the presence of the DM interaction, the thermal Hall effect of magnons is prohibited by symmetry, as confirmed by experiments.[46]

Another interaction to induce a nonzero Berry curvature is the dipolar interaction.[18,25] The dipolar interaction is a classical interaction between the magnetic moments $\mathbf{m}_1$ and $\mathbf{m}_2$ at $\mathbf{r}_1$ and $\mathbf{r}_2$, described by

$$H = -\frac{\mu_0}{4\pi|\mathbf{r}_1-\mathbf{r}_2|^3}\left[\frac{3\mathbf{m}_1\cdot(\mathbf{r}_1-\mathbf{r}_2)\mathbf{m}_2\cdot(\mathbf{r}_1-\mathbf{r}_2)}{|\mathbf{r}_1-\mathbf{r}_2|^2} - \mathbf{m}_1\cdot\mathbf{m}_2\right]. \tag{39}$$

This depends not only on the orientations of the magnetic moments $\mathbf{m}_1$ and $\mathbf{m}_2$ but also on the relative positions of the two magnetic moments; thereby, it works as a "spin–orbit interaction" of spins.

This dipolar interaction inversely scales with the cube of the distance between the dipoles and is quasi-long-ranged. It is in contrast with the short-ranged nature of the exchange interaction. Hence, in spin systems with both exchange and dipolar interactions, the dominant interaction depends on the wavelength of the spin wave considered. At long wavelengths (∼μm), the dipolar interaction is dominant, and this magnon is called a magnetostatic wave.[47–49] On the other hand, at short wavelengths (∼nm), the exchange interaction is dominant, and the Berry curvature is expected to be small when the DM interaction is absent. In the following, we consider the Berry curvature for the magnon, induced by the DM and dipolar interactions. The formalism of the magnon Berry curvature for the DM interaction is similar to that in electronic systems. Moreover, that for the dipolar interaction is different. Because the dipolar interaction is longer ranged, the magnons are sensitive to the sample shape. In order to incorporate the dipolar interaction with these peculiar properties, the theoretical treatment is different from that for electronic systems, and we extensively explain this procedure in detail in Sects. 4.2 and 4.3.

4.1 Berry curvature induced by DM interaction

The DM interaction has the form $\boldsymbol{D}\cdot(\boldsymbol{S}_i\times\boldsymbol{S}_j)$ between the spins $\boldsymbol{S}_i$ and $\boldsymbol{S}_j$. The vector $\boldsymbol{D}$ is called a DM vector, and its direction depends on the symmetry of the crystal. In particular, when the crystal has an inversion symmetry with respect to the midpoint of the bond between $\boldsymbol{S}_i$ and $\boldsymbol{S}_j$, the DM interaction is absent. Therefore, to see the effects due to the DM interaction, one should choose materials with an appropriate lattice structure. In general, in the presence of the DM interaction $\boldsymbol{D}\cdot(\boldsymbol{S}_i\times\boldsymbol{S}_j)$, together with the exchange interaction, the neighboring spins prefer to have a nonzero angle between them, rather than to be parallel. Thus, the ground states of magnets with the DM interaction often have a spiral or conical spin structure. Although magnons in such spiral or conical magnets are expected to have a nonzero Berry curvature, their analysis is complicated. On the other hand, $Lu_2V_2O_7$ is a collinear ferromagnet in the presence of the DM interaction and its theoretical treatment is easier. Therefore, in the following, we explain this ferromagnet in detail.[17]

$Lu_2V_2O_7$ has a pyrochlore structure, and nearest-neighbor bonds lack an inversion center, leading to a nonzero DM interaction. Nevertheless, its ground state is a collinear ferromagnet, rather than a spiral or conical spin texture, because for each site in the ferromagnetic ground state, the DM interactions from the neighboring spins cancel each other. On the other hand, the magnon spectrum is affected by the DM interaction, giving rise to the nonzero Berry curvature. Indeed, the thermal Hall effect has been measured and analyzed in Ref. 17, as shown in Fig. 3(a). The spin Hamiltonian is written as

$$H_{\rm eff}=\sum_{\langle i,j\rangle}-J\boldsymbol{S}_i\cdot\boldsymbol{S}_j+\boldsymbol{D}_{ij}\cdot(\boldsymbol{S}_i\times\boldsymbol{S}_j)-g\mu_{\rm B}\boldsymbol{H}\cdot\sum_i\boldsymbol{S}_i,$$

where $\langle i,j\rangle$ denotes the nearest neighbor pairs, J is the exchange interaction, g is the g-factor, $\mu_{\rm B}$ is the Bohr magneton, and $\boldsymbol{H}$ is the magnetic field.[17] From this spin Hamiltonian, one can derive a Hamiltonian for magnons, with magnon–magnon interaction terms. To simplify the analysis, we focus on the temperature region much lower than the Curie temperature, and the magnon–magnon interactions are neglected here. The hopping terms of magnons then have the form $J+iD_{ij}$, where $D_{ij}=\boldsymbol{D}_{ij}\cdot\boldsymbol{H}/|\boldsymbol{H}|$. Since this hopping term is complex, its phase serves as an orbital magnetic field for magnons, which naturally leads to a nonzero Berry curvature and a Hall effect. We focus on the lowest mode of magnons, because it gives a dominant contribution to the thermal Hall conductivity at low temperatures. As a result, the lowest magnon band in the vicinity of $k=0$ has a dispersion $\varepsilon_{1\boldsymbol{k}}\sim 2JSA^2k^2+g\mu_{\rm B}H$ and the jth component of its Berry curvature is calculated as

$$\Omega_{1,j}\simeq-\frac{A^4}{8\sqrt{2}}\frac{D}{J}\frac{H_j}{H}(k^2+k_j^2),$$

where $4A$ is a lattice constant of the cubic unit cell. From this Berry curvature, one can calculate the thermal Hall conductivity κ_{xy}. The broken curve in Fig. 3(b) shows a theoretical result of the magnon thermal Hall conductivity obtained in Ref. 17. It is calculated only for the $S_{ij}^{\alpha\beta}$ term in Eq. (28). As presented in the previous section, one should include the $M_{ij}^{\alpha\beta}$ term as well; the correct result, given by $S_{ij}^{\alpha\beta}+M_{ij}^{\alpha\beta}$, is shown as a solid curve in Fig. 3(b).[25] This solid curve agrees well with the experiment shown in Fig. 3(a).

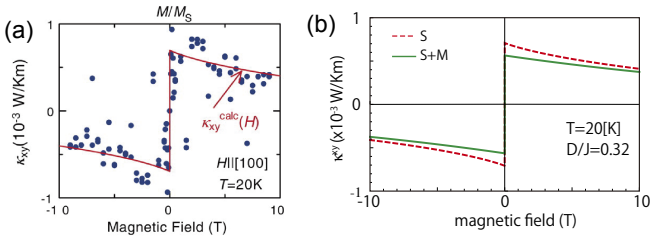

Fig. 3. (Color online) (a) Experimental and theoretical results for the magnon thermal Hall conductivity in $Lu_2V_2O_7$ and (b) thermal Hall conductivity in the magnetic field.[25] In (a), the dots are experimental results, and the curve represents a theoretical result, only from the $S_{ij}^{\alpha\beta}$ term. In (b), the solid and broken curves indicate $S_{ij}^{\alpha\beta}+M_{ij}^{\alpha\beta}$ and $S_{ij}^{\alpha\beta}$ in the calculation, respectively, and therefore the broken line in (b) is identical to the curve in (a). (a) is adapted with permission from Ref. 17. © 2010 American Association for the Advancement of Science.

4.2 Dispersion of magnetostatic wave

One of the peculiar characteristics of the dipolar interaction is the sensitivity to sample shape. It stems from the quasi-long-ranged nature of the dipolar interaction. This sample-shape dependence appears also in dispersions of spin waves. Let us take a ferromagnetic film (see Fig. 4) as an example. We apply an external magnetic field to fix magnetization direction at equilibrium, without the formation of complex magnetic domains. The spin-wave excitations depend on the directions of the saturation magnetization $\mathbf{M}_0$ and the wavevector $\mathbf{k}$ of the spin waves, and have been well studied since the 1960s.[48,49] We set the coordinate systems $\xi\eta\zeta$ and xyz, as shown in Fig. 5. The film is infinite along the η- and ζ-directions, and has a finite width along the ξ-direction. The ζ-axis is taken to be along the magnon wave vector $\mathbf{k}$. On the

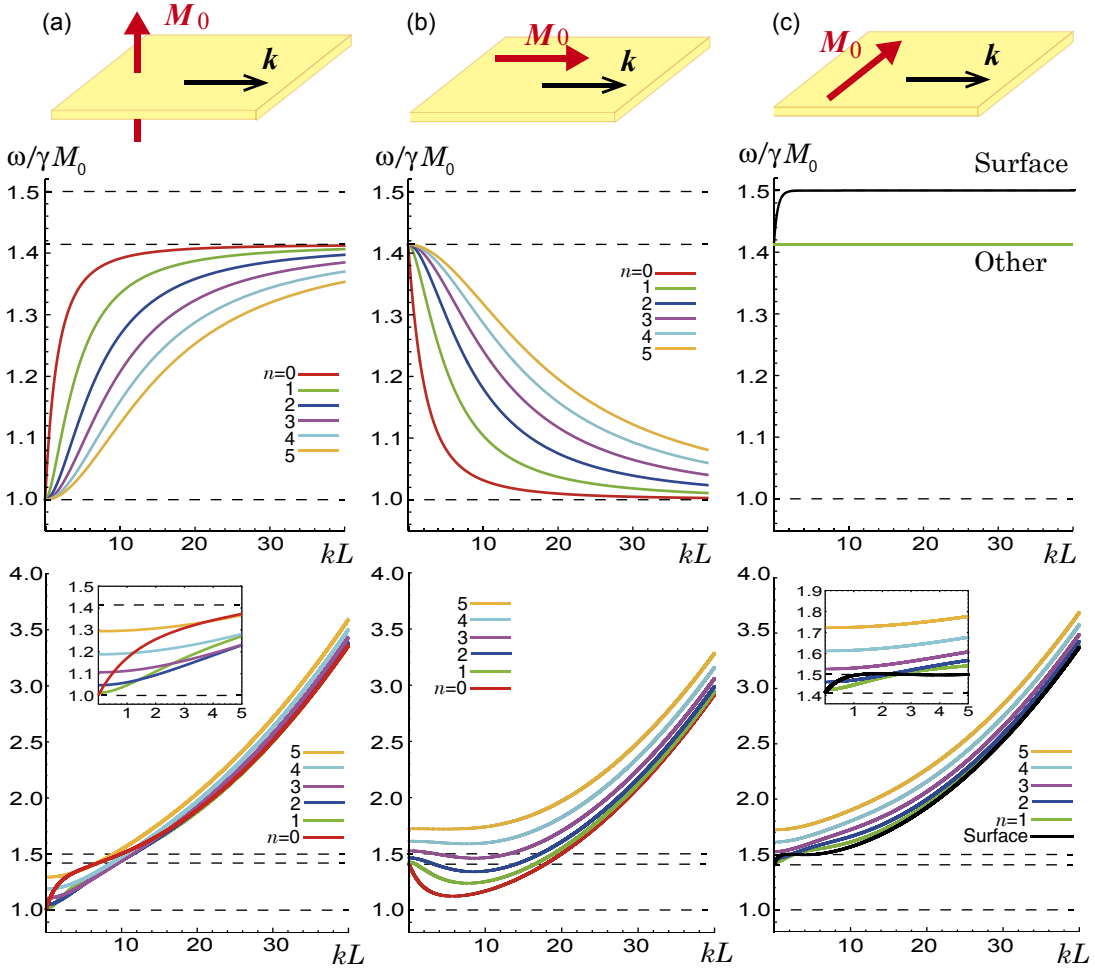

Fig. 4. (Color online) (Top panels) Schematic figures of the magnetization and the wavevector of magnetostatic waves in the magnetic film for (a) MSFVW mode [$\mathbf{M}_0$ is perpendicular to the film ($\theta = 0$)], (b) MSBVW mode [$\mathbf{M}_0(\parallel \mathbf{k})$ in the film ($\theta = 90°$ and $\varphi = 0$)], and (c) MSSW mode [$\mathbf{M}_0(\perp \mathbf{k})$ in the film ($\theta = 90°$ and $\varphi = 90°$)]. The middle panels show the dispersions for magnets with dipole interactions only, and the bottom panels show those for magnets with dipole and exchange interactions. Each dispersion is calculated for $H_0/M_0 = 1$ where H_0 is the external magnetic field, M_0 is the spontaneous magnetization, and L is the film thickness. The unpinned boundary conditions for both surfaces are adopted. The parameters used in the plots are given in the text.

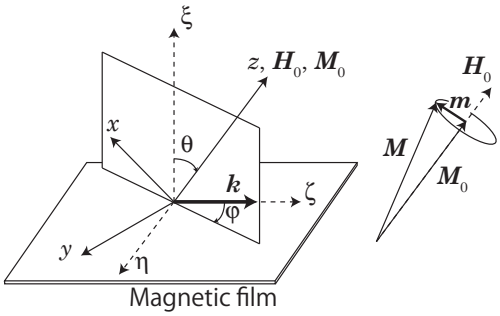

Fig. 5. Geometry of the coordinate axes. The magnetization $\mathbf{M}$ precesses around $\mathbf{M}_0$. The ζ-axis is taken to be along the wavevector $\mathbf{k}$.

other hand, the z-axis is taken to be along both the saturation magnetization $\mathbf{M}_0$ and the internal static magnetic field $\mathbf{H}_0$. The angular coordinates θ and φ are defined as shown in Fig. 5, following Ref. 50. Depending on the directions of the saturation magnetization $\mathbf{M}_0$ and the wave vector $\mathbf{k}$, there are three typical eigenmodes: (a) $\mathbf{M}_0$ is perpendicular to the film ($\theta = 0$), (b) $\mathbf{M}_0 \parallel \mathbf{k}$ in the film ($\theta = 90°$ and $\varphi = 0$), and (c) $\mathbf{M}_0 \perp \mathbf{k}$ in the film ($\theta = 90°$ and $\varphi = 90°$) (see top panels in Fig. 4). These modes are called (a) magnetostatic forward volume-wave (MSFVW) mode, (b) magnetostatic backward volume-wave (MSBVW) mode, and (c) magnetostatic surface-wave (MSSW) mode, respectively. The MSSW mode is localized near one of the surfaces of the film. The MSFVW (MSBVW) mode has a positive (negative) group velocity within the wavelength range of μm where the dipolar interaction is dominant. The dispersions of the three modes are depicted in the middle of Fig. 4 in a case with only a dipolar interaction. In the figure, only the lowest six modes are shown.

It is not straightforward to formulate the Berry curvature of the magnetostatic waves using the complicated form of the dipolar interaction in Eq. (39). As an alternative method, here, we use the formulation of magnetostatic waves as an eigenvalue problem in Ref. 50. We put the spin wave as $\mathbf{m}(\xi, \zeta, t) = \mathbf{m}(\xi) \exp(i(k\zeta - \omega t))$, with a two-dimensional vector $\mathbf{m}(\xi) = \begin{pmatrix} m_x(\xi) \\ m_y(\xi) \end{pmatrix}$, which is perpendicular to $\mathbf{M}_0$. Then, the equation of motion of the magnetization is constructed using the linearized Landau–Lifshitz equation $\partial \mathbf{m}/\partial t = -\gamma(\mathbf{m} \times \mathbf{H})$ with the Maxwell equation in the magnetostatic limit $\nabla \times \mathbf{H} = 0$, $\nabla \cdot \mathbf{B} = 0$, and the usual boundary conditions for $\mathbf{H}$ and $\mathbf{B}$. Here, γ is the gyromagnetic ratio.

By taking into account the dipolar interaction and an isotropic exchange interaction αk^2 (α: exchange constant), the linearized Landau–Lifshitz equation is rewritten into the following integral equation:[50]

$$\hat{N}\mathbf{m}(\xi) - \int_{-L/2}^{L/2} \hat{G}(\xi,\xi')\mathbf{m}(\xi')\,d\xi' = \frac{\omega}{\omega_M}\sigma_y \mathbf{m}(\xi), \tag{40}$$

where we use the SI units, L is the film thickness, $\sigma_y = \left(\begin{smallmatrix} 0 & -i \\ i & 0 \end{smallmatrix}\right)$ is the Pauli matrix, $\omega_H = \gamma H_0$, and $\omega_M = \gamma M_0$. $\hat{G}(\xi,\xi')$ is the 2×2 complex matrix of Green's function:

$$\hat{G}(\xi,\xi') = \begin{pmatrix} G_{xx} & G_{xy} \\ G_{yx} & G_{yy} \end{pmatrix}, \tag{41}$$

$$G_{xx} = (G_P - \delta(\xi-\xi'))\sin^2\theta - iG_Q \sin 2\theta \cos\varphi - G_P \cos^2\theta\cos^2\varphi, \tag{42}$$

$$G_{xy} = G_{yx} = -iG_Q \sin\theta\sin\varphi - G_P\cos\theta\sin\varphi\cos\varphi, \tag{43}$$

$$G_{yy} = -G_P \sin^2\varphi, \tag{44}$$

where

$$G_P = \frac{k}{2}\exp(-k|\xi-\xi'|), \quad G_Q = G_P\,\mathrm{sign}(\xi-\xi'). \tag{45}$$

The operator $\hat{N}$ is defined as

$$\hat{N} = \left(-\alpha\frac{\partial^2}{\partial\xi^2} + \alpha k^2 + \frac{\omega_H}{\omega_M}\right)\hat{I}, \quad \hat{I} = \begin{pmatrix} 1 & 0 \\ 0 & 1 \end{pmatrix}. \tag{46}$$

In Fig. 4, we show dispersions with the parameters $\omega_H = \omega_M = 5.0\,\mathrm{GHz}$ and $L = 0.51\times 10^{-4}\,\mathrm{cm}$. In Eq. (40), the boundary conditions at both surfaces should be specified, and here, for simplicity, we consider unpinned boundary conditions at the top and bottom surfaces. In the middle panels of Fig. 4, we show the cases with dipolar interactions only ($\alpha = 0$), and in the bottom panels, we show the cases with dipolar and exchange interactions with $\alpha = 3.1\times 10^{-12}\,\mathrm{cm}^2$. We can see that the dispersion with only a dipolar interaction has degeneracy at $\mathbf{k} = 0$. The exchange interaction lifts the degeneracy at $\mathbf{k} = 0$ and gives a parabolic dispersion ($\sim\alpha k^2$) for a large $\mathbf{k}$.

Equation (40) is not a simple eigenvalue equation but a generalized one due to the presence of σ_y. This is physically due to the precessional nature of the motion, as we show in the following. By a unitary transformation, the equation of motion is rewritten as

$$\hat{N}\mathbf{m}'(\xi) - \int_{-L/2}^{L/2} \hat{G}'(\xi,\xi')\mathbf{m}'(\xi')\,d\xi' = \frac{\omega}{\omega_M}\sigma_z \mathbf{m}'(\xi), \tag{47}$$

$$\sigma_z \equiv \begin{pmatrix} 1 & 0 \\ 0 & -1 \end{pmatrix}, \quad \mathbf{m}'(\xi) \equiv \frac{1}{\sqrt{2}}\begin{pmatrix} m_x(\xi) - im_y(\xi) \\ m_x(\xi) + im_y(\xi) \end{pmatrix}.$$

$\hat{G}'(\xi,\xi')$ is the 2×2 matrix of Green's function after the unitary transformation from $\hat{G}$. Physically, the precession motion is roughly described as $m_x \sim \cos\omega t$, $m_y \sim -\sin\omega t$, i.e., $m_x \pm im_y \sim e^{\mp i\omega t}$, and the two components of $\mathbf{m}'$ oscillate with frequencies with opposite signs, $+\omega$ and $-\omega$. Thus, the emergence of σ_z is natural for this kind of precession motion. Note that Eq. (47) is of the BdG Hamiltonian form by casting it to a second-quantized form.[35]

4.3 *Berry curvature of magnetostatic wave*

Since Eq. (40) in the magnetostatic limit is a generalized eigenvalue problem, we have to modify the prescription of our theory of the Berry curvature. The Berry curvature is now written as

$$\Omega_{n,\gamma}(\mathbf{k}) = i\epsilon_{\alpha\beta\gamma}\left\langle \frac{\partial \mathbf{m}_{n,\mathbf{k}}}{\partial k_\alpha}\middle|\sigma_y\middle|\frac{\partial \mathbf{m}_{n,\mathbf{k}}}{\partial k_\beta}\right\rangle, \tag{48}$$

where $\epsilon_{\alpha\beta\gamma}$ is the antisymmetric tensor. Here, the wavefunction is normalized as

$$\langle \mathbf{m}_{n,\mathbf{k}}|\sigma_y|\mathbf{m}_{n,\mathbf{k}}\rangle = 1. \tag{49}$$

We note that this definition of the Berry curvature is the same as that in Eq. (36). From this definition, the Berry curvature vanishes when the saturation magnetization $\mathbf{M}_0$ lies in the film ($\theta = \pi/2$), i.e., for the MSBVW and MSSW modes, owing to the symmetry of the system.[18] On the other hand, the Berry curvature is nonzero in the MSFVW mode, in which the saturation magnetization is perpendicular to the film ($\theta = 0$).

In the following discussion, for simplicity, we consider the case with a dipolar interaction only; thereby, the Berry curvature can be evaluated analytically. In the following, we calculate the Berry curvature for the MSFVW mode at $\theta = 0$, and thus the ξ-direction is parallel to the z-direction. The solution of the integral equation [Eq. (40)] of the nth band without an exchange interaction ($\alpha = 0$) for $\theta = 0$ is written as[48]

$$\mathbf{m}_{n\mathbf{k}}(z) = \begin{pmatrix} m^x_{n\mathbf{k}}(z) \\ m^y_{n\mathbf{k}}(z) \end{pmatrix} \propto \begin{pmatrix} i\kappa k_x + \nu k_y \\ -\nu k_x + i\kappa k_y \end{pmatrix}\cos\left(\sqrt{p}kz + \frac{n\pi}{2}\right), \tag{50}$$

where $\kappa = \omega_M\omega_H/(\omega_H^2 - \omega_n^2)$, $\nu = \omega_M\omega_n/(\omega_H^2 - \omega_n^2)$, and $p = -1 - \kappa > 0$. Here, the nth eigenmode frequency ω_n for $n = 0, 1, 2, \ldots$ is determined as

$$\sqrt{p}\tan\left(\frac{\sqrt{p}kL + n\pi}{2}\right) = 1. \tag{51}$$

By substituting this solution into Eq. (48), the Berry curvature for the nth MSFVW mode is written as

$$\Omega_{n,z}(\mathbf{k}) = \frac{1}{2\omega_H}\frac{1}{k}\frac{\partial\omega_n}{\partial k}\left(1 - \frac{\omega_H^2}{\omega_n^2}\right). \tag{52}$$

Figures 6(a) and 6(b) show the numerical results of the dispersion and the Berry curvature calculated from Eqs. (51) and (52) in the case with $H_0 = M_0$. Here we show only the curvature for the particle bands. We find that $\Omega_{n,z}(\mathbf{k} = 0) = 0$ for the $n > 0$ mode, and that for the $n = 0$ mode, $\Omega_{0,z}(\mathbf{k})$ converges at a constant at $k = 0$.

From this Berry curvature, we can calculate the thermal Hall conductivity for the MSFVW mode.[35] For $k_\mathrm{B}T \gg \hbar\omega_H$, which holds true in realistic cases (e.g., when $T = 300\,\mathrm{K}$ and $H_0 = 1\,\mathrm{T}$ in YIG films, $k_\mathrm{B}T/\hbar\omega_H = 1.5\times 10^5$), we can estimate the thermal Hall conductivity as

$$\kappa_{xy} \simeq \frac{k_\mathrm{B}\omega_M N}{8\pi}\left(1 - r\log\left(1 + \frac{1}{r}\right)\right), \tag{53}$$

where $r \equiv H_0/M_\mathrm{s}$. Here, $N = L/l_\mathrm{ex}$ is the ratio between the exchange length l_ex and film thickness L. Thus, the thermal Hall conductivity via the MSFVW is almost independent of the temperature for $k_\mathrm{B}T \gg \hbar\omega_H$. From the exchange length

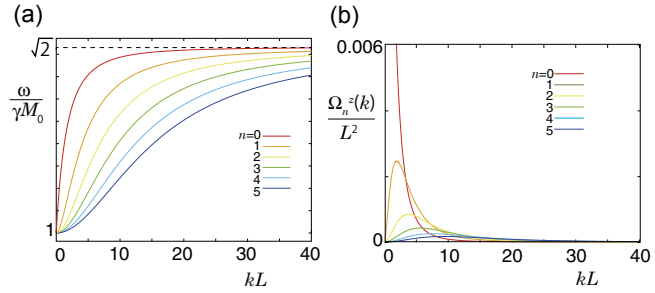

Fig. 6. (Color online) (a) Dispersion and (b) Berry curvature for the MSFVW mode for $H_0/M_0 = 1.0$. Only the dipolar interaction is considered.

$l_{ex} = 1.72 \times 10^{-8}$ m for the YIG film, it is evaluated as $\kappa_{xy}/L = 5.9 \times 10^{-8}\,\mathrm{W\,K^{-1}\,m^{-1}}$, where parameters are set as $\gamma = 2.8$ MHz/Oe, $M_s = 1750$ G, $T = 300$ K, and $H_{ex} = 3000$ Oe. It is almost temperature independent above $\hbar\omega_H/k_B \sim 27$ mK. Nevertheless, it might be very small for experimental observations.

4.4 Further theoretical works on thermal Hall effect

The formula of the magnon thermal Hall effect is widely applicable to any noninteracting bosons. It has been applied to a ferromagnet on a Kagome lattice[51] and a Skyrmion lattice,[52] to study the behaviors of the thermal Hall conductivity. In particular, in Ref. 51 the temperature and the field dependence of the thermal Hall effect in $Lu_2V_2O_7$ are theoretically studied and compared with measurements by Onose et al.[17]

The magnon band structure and its Berry curvature can be designed by the spatial modulation of the magnet. In particular, by introducing periodicity into a magnet to obtain a magnonic crystal, the Berry curvature due to a dipolar interaction can be enhanced. The periodicity can be designed in such a way that the Chern numbers for individual bands can be nonzero; it can be called a topological magnonic crystal.[36–38] Furthermore, we note that a plateau–plateau transition in a disordered topological magnonic crystal with a dipolar interaction is studied,[53] analogous to that in the integer quantum Hall effect.

As an example of a topological magnonic crystal, in Ref. 36, a two-dimensional lattice of magnetic cylindrical nanopillars embedded in another magnetic material is considered. The wavelength and spatial periodicity of the magnonic crystal for magnetostatic waves are of micrometer order, which might be experimentally realizable in the future. We note that similar kinds of edge modes in a two-dimensional array of dipolarly coupled magnetic nanopillars are discussed in Refs. 54 and 55. Although the geometries in Refs. 54 and 55 resemble that in Ref. 36 in that dipolarly coupled cylinders are forming a square lattice, the edge modes in Refs. 54 and 55 do not seem to originate from the mechanism proposed in Ref. 36, i.e., a topological origin due to a nonzero Chern number. This is because these edge modes in Refs. 54 and 55 lie above the bulk bands. In contrast, topological edge modes from a nonzero Chern number should always appear between bulk bands.

We note that topological chiral edge modes are also realized in a tight-binding model on a Kagome lattice with exchange and DM interactions, as first shown in Ref. 43. For the Kagome lattice model, the dependences of the band structure and Chern numbers of the bands on various parameters have been investigated in Refs. 43, 51, and 56. Furthermore, topological chiral modes at the interfaces of nontrivial topological phases in the Kagome lattice model are studied, particularly magnon dispersions and the bulk-boundary correspondence,[57] as well as their transport properties.[58] Topological edge modes on another tight-binding model, constructed on a Lieb lattice with a DM interaction, are also investigated.[59]

Thus far, we have adopted a noninteracting picture of magnons. In some ferromagnets on geometrically frustrated lattices, the interaction between magnons gives rise to appreciable damping, as demonstrated in the $S = 1/2$ ferromagnet on the kagome lattice.[60] In this system, the interaction between magnons gives rise to nonperturbative damping as large as the magnon bandwidth, and a framework based on noninteracting magnons breaks down.

Apart from the bosonic description of the magnon Hall effect discussed here, the theoretical formulation of the thermal Hall effect in terms of spin operators (not with bosons) has also been developed.[61] The theory presented in Sect. 3 deals with bosonic systems, by using the bosonic Hamiltonian with interaction between bosons neglected. By the Holstein–Primakoff transformation, there appear many terms for the interaction between bosons, and it is unclear whether they can be ignored. In this sense, the approach in Ref. 61 gives an alternative route for the thermal Hall effect of magnons, entirely by the spin language. By this formalism, the emergence of the thermal Hall effect even in a paramagnetic phase under a magnetic field is theoretically shown.[61]

5. Conclusions

For the observation of the magnon Hall effect for magnetostatic waves, it is straightforward to measure the thermal Hall effect. Nevertheless, the thermal Hall conductivity of magnetostatic waves for the realisitic parameters is very small for experimental observation. On the other hand, for magnons with the DM interactions, the thermal Hall effect becomes larger in some magnets, and a comparison between theories and experiments has been made to show good agreement.[17,46]

Another method of measuring for the thermal Hall effect can be proposed from the semiclassical theory. The Berry curvature in Eq. (7) survives only when $\dot{\mathbf{k}}$ is nonzero. To have this effect, we can consider a reflection of the magnon wavepacket at the edge of a two-dimensional magnet, such as a ferromagnetic slab. Then, the $-\dot{\mathbf{k}} \times \boldsymbol{\Omega}_n(\mathbf{k})$ term is along the edge of the magnet, and it results in the shift of the wavepacket along the edge at the reflection. If the direction of the magnetic field is reversed, the Berry curvature changes its sign, and the shift is also reversed (see Fig. 7). The motions of magnon wavepackets can be observed by several methods. Besides the Brillouin light scattering,[11] one can easily see them by infrared imaging as a temperature distribution. In Ref. 62, a magnon wavepacket is injected onto the edge, and the temperature gradient along the edge is observed by infrared imaging. This observed temperature gradient might be regarded as a shift due to the Berry curvature.

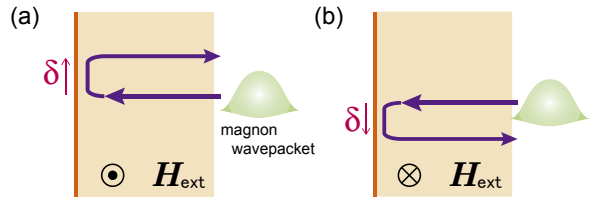

Fig. 7. (Color online) Schematic illustration of the reflections of the magnon wavepacket at the edge, with opposite magnetic fields.

Furthermore, the temperature distribution along the edge is reversed as the magnetic field is reversed. This agrees with the expectations of the magnon Hall effect.

The theory of the thermal Hall effect in this paper can also be applied to other bosonic excitations in magnets. For example, a triplon excitation in $SrCu_2(BO_3)_2$ in a magnetic field is studied theoretically. This magnet is theoretically interesting since it realizes the Shastry–Sutherland model, with a small anisotropy from a DM interaction. In this model, topological edge modes similar to those in quantum Hall systems and the thermal Hall effect are predicted theoretically.[63] Furthermore, in the magnet Cu(1,3-bdc)[64] having a Kagome lattice with a DM interaction, the thermal Hall effect is experimentally found to show sign reversal with changes in temperature or magnetic field, precluding a phonon origin of the thermal Hall effect.

The thermal Hall effect can also be a useful probe for unveiling the properties of unknown magnetic excitations. In the quantum spin-ice system $Tb_2Ti_2O_7$,[65] a high thermal Hall conductivity is observed. Since this material does not have long-range order at the temperature of the measurement due to frustration, the nature of spin excitation is yet to be understood. The measured signal is similar to that of a disordered metal, implying that the thermal Hall effect can be a useful probe for investigating the properties of spin excitations.

To summarize, the thermal Hall effect can be promising as a new type of probe for magnetism and magnetic excitations, because it is concerned with different types of physics than other probes. In addition, transverse transport, as compared with longitudinal transport, is free from parasitic effects by, for example, phonons. In transverse responses such as the thermal Hall effect, there are not many other effects superposed onto the signal, and thereby a comparison between experiments and theories is easier. Thus, the thermal Hall effect can be a promising candidate probe of magnetism. On the theoretical side, there is also much room for additional investigations, such as those on the interaction effect between magnons, the relationship between spin and boson languages, theoretical designs for enhanced magnon Hall effects, and realistic proposals for topological magnonic edge modes.

Acknowledgments

We would like to thank R. Matsumoto, R. Shindou, J. Ohe, E. Saitoh, K. Tanabe, T. Moriyama, D. Chiba, K. Kobayashi, and T. Ono for fruitful collaborations, on which the present work is partly based. This work was partly supported by a Grant-in-Aid for Scientific Research on Innovative Areas, "Nano Spin Conversion Science" (Grant No. 26100006).

*murakami@stat.phys.titech.ac.jp

1) F. Bloch, Z. Phys. **61**, 206 (1930).
2) C. Kittel, Phys. Rev. **73**, 155 (1948).
3) S. A. Wolf, D. D. Awschalom, R. A. Buhrman, J. M. Daughton, S. von Molnar, M. L. Roukes, A. Y. Chtchelkanova, and D. M. Treger, Science **294**, 1488 (2001).
4) D. Grundler, Phys. World **15**, 39 (2002).
5) V. V. Kruglyak and R. J. Hicken, J. Magn. Magn. Mater. **306**, 191 (2006).
6) S. Neusser, B. Botters, and D. Grundler, Phys. Rev. B **78**, 054406 (2008).
7) A. A. Serga, A. V. Chumak, and B. Hillebrands, J. Phys. D **43**, 264002 (2010).
8) B. Lenk, H. Ulrichs, F. Garbs, and M. Münzenberg, Phys. Rep. **507**, 107 (2011).
9) O. Büttner, M. Bauer, A. Rueff, S. O. Demokritov, B. Hillebrands, A. N. Slavin, M. P. Kostylev, and B. A. Kalinikos, Ultrasonics **38**, 443 (2000).
10) Y. Kajiwara, K. Harii, S. Takahashi, J. Ohe, K. Uchida, M. Mizuguchi, H. Umezawa, H. Kawai, K. Ando, K. Takanashi, S. Maekawa, and E. Saitoh, Nature **464**, 262 (2010).
11) S. O. Demokritov, B. Hillebrands, and A. N. Slavin, Phys. Rep. **348**, 441 (2001).
12) M.-C. Chang and Q. Niu, Phys. Rev. B **53**, 7010 (1996).
13) G. Sundaram and Q. Niu, Phys. Rev. B **59**, 14915 (1999).
14) D. J. Thouless, M. Kohmoto, M. P. Nightingale, and M. den Nijs, Phys. Rev. Lett. **49**, 405 (1982).
15) D. Xiao, M.-C. Chang, and Q. Niu, Rev. Mod. Phys. **82**, 1959 (2010).
16) H. Katsura, N. Nagaosa, and P. A. Lee, Phys. Rev. Lett. **104**, 066403 (2010).
17) Y. Onose, T. Ideue, H. Katsura, Y. Shiomi, N. Nagaosa, and Y. Tokura, Science **329**, 297 (2010).
18) R. Matsumoto and S. Murakami, Phys. Rev. Lett. **106**, 197202 (2011).
19) M. Onoda, S. Murakami, and N. Nagaosa, Phys. Rev. Lett. **93**, 083901 (2004).
20) M. V. Berry, Proc. R. Soc. London, Ser. A **392**, 45 (1984).
21) S. Murakami, N. Nagaosa, and S. C. Zhang, Science **301**, 1348 (2003).
22) J. Sinova, D. Culcer, Q. Niu, N. A. Sinitsyn, T. Jungwirth, and A. H. MacDonald, Phys. Rev. Lett. **92**, 126603 (2004).
23) M. Kohmoto, Ann. Phys. (N.Y.) **160**, 343 (1985).
24) K. Yu. Bliokh and Y. P. Bliokh, Phys. Rev. Lett. **96**, 073903 (2006).
25) R. Matsumoto and S. Murakami, Phys. Rev. B **84**, 184406 (2011).
26) L. Smrčka and P. Středa, J. Phys. C **10**, 2153 (1977).
27) H. Oji and P. Středa, Phys. Rev. B **31**, 7291 (1985).
28) D. L. Bergman and V. Oganesyan, Phys. Rev. Lett. **104**, 066601 (2010).
29) D. Xiao, J. Shi, and Q. Niu, Phys. Rev. Lett. **95**, 137204 (2005).
30) T. Thonhauser, D. Ceresoli, D. Vanderbilt, and R. Resta, Phys. Rev. Lett. **95**, 137205 (2005).
31) D. Xiao, Y. Yao, Z. Fang, and Q. Niu, Phys. Rev. Lett. **97**, 026603 (2006).
32) L. M. Luttinger, Phys. Rev. **135**, A1505 (1964).
33) T. Qin, Q. Niu, and J. Shi, Phys. Rev. Lett. **107**, 236601 (2011).
34) G. Tatara, Phys. Rev. B **92**, 064405 (2015).
35) R. Matsumoto, R. Shindou, and S. Murakami, Phys. Rev. B **89**, 054420 (2014).
36) R. Shindou, R. Matsumoto, S. Murakami, and J. Ohe, Phys. Rev. B **87**, 174427 (2013).
37) R. Shindou, J. Ohe, R. Matsumoto, S. Murakami, and E. Saitoh, Phys. Rev. B **87**, 174402 (2013).
38) R. Shindou and J. Ohe, Phys. Rev. B **89**, 054412 (2014).
39) O. Vafek, A. Melikyan, and Z. Tešanović, Phys. Rev. B **64**, 224508 (2001).
40) K. Nomura, S. Ryu, A. Furusaki, and N. Nagaosa, Phys. Rev. Lett. **108**, 026802 (2012).
41) H. Sumiyoshi and S. Fujimoto, J. Phys. Soc. Jpn. **82**, 023602 (2013).
42) J. H. P. Colpa, Physica A **93**, 327 (1978).
43) L. Zhang, J. Ren, J.-S. Wang, and B. Li, Phys. Rev. B **87**, 144101 (2013).
44) R. Cheng, S. Okamoto, and D. Xiao, arXiv:1606.01952.
45) V. A. Zyuzin and A. A. Kovalev, arXiv:1606.03088.
46) T. Ideue, Y. Onose, H. Katsura, Y. Shiomi, S. Ishiwata, N. Nagaosa, and Y. Tokura, Phys. Rev. B **85**, 134411 (2012).

47) L. R. Walker, J. Appl. Phys. **29**, 318 (1958).
48) R. W. Damon and H. van de Vaart, J. Appl. Phys. **36**, 3453 (1965).
49) R. W. Damon and J. R. Eshbach, J. Phys. Chem. Solids **19**, 308 (1961).
50) B. A. Kalinikos and A. N. Slavin, J. Phys. C **19**, 7013 (1986).
51) A. Mook, J. Henk, and I. Mertig, Phys. Rev. B **89**, 134409 (2014).
52) K. A. van Hoogdalem, Y. Tserkovnyak, and D. Loss, Phys. Rev. B **87**, 024402 (2013).
53) B. Xu, T. Otsuki, and R. Shindou, arXiv:1606.02839.
54) I. Lisenkov, V. Tyberkevych, A. Slavin, P. Bondareno, B. A. Ivanov, E. Bankowski, T. Meitzler, and S. Nikitov, Phys. Rev. B **90**, 104417 (2014).
55) I. Lisenkov, V. Tyberkevych, S. Nikitov, and A. Slavin, Phys. Rev. B **93**, 214441 (2016).
56) A. Mook, J. Henk, and I. Mertig, Phys. Rev. B **90**, 024412 (2014).
57) A. Mook, J. Henk, and I. Mertig, Phys. Rev. B **91**, 224411 (2015).
58) A. Mook, J. Henk, and I. Mertig, Phys. Rev. B **91**, 174409 (2015).
59) X. Cao, K. Chen, and D. He, J. Phys.: Condens. Matter **27**, 166003 (2015).
60) A. L. Chernyshev and P. A. Maksimov, Phys. Rev. Lett. **117**, 187203 (2016).
61) H. Lee, J. H. Han, and P. A. Lee, Phys. Rev. B **91**, 125413 (2015).
62) K. Tanabe, R. Matsumoto, J. Ohe, S. Murakami, T. Moriyama, D. Chiba, K. Kobayashi, and T. Ono, Phys. Status Solidi B **253**, 783 (2016).
63) J. Romhányi, K. Penc, and R. Ganesh, Nat. Commun. **6**, 6805 (2015).
64) M. Hirschberger, R. Chisnell, Y. S. Lee, and N. P. Ong, Phys. Rev. Lett. **115**, 106603 (2015).
65) M. Hirschberger, J. W. Krizan, R. J. Cava, and N. P. Ong, Science **348**, 106 (2015).

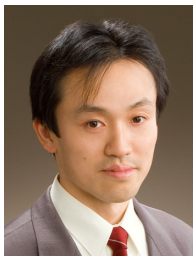

Shuichi Murakami was born in Osaka, Japan in 1970. He graduated in Physics (1993) at the University of Tokyo. He obtained his Ph.D. (1999) degree from the University of Tokyo. He was research associate (1995–2007) at the Department of Applied Physics, University of Tokyo. He moved to Tokyo Institute of Technology as associate professor in 2007, and became professor in the Department of Physics and in the Materials Research Center for Element Strategy in 2012. In 2003, in collaboration with Professor N. Nagaosa and Professor S.-C. Zhang, he theoretically proposed intrinsic spin Hall effect, which has been observed experimentally later. Since then he has been working on theories of spintronics and topological phases in condensed matter physics. He received Young Scientist Award of the Physical Society of Japan in 2007, Young Scientists' Prize of the Commendation for Science and Technology by the Minister of Education, Culture, Sports, Science and Technology and Sir Martin Wood Prize in 2010, IBM Japan Science Prize in 2011, and JSPS Prize in 2012.

Akihiro Okamoto was born in Aichi Prefecture, Japan in 1989. He obtained his B.Sc. (2013) and M.Sc. (2015) degrees from Tokyo Institute of Technology. Since 2015, he has been a Ph.D. student in the Department of Physics, Tokyo Institute of Technology. His research field is Berry curvature of spin waves in ferromagnetic films.